The effect of metal oxide decorated graphene hybrids on the improved thermal stability and the reduced smoke toxicity in epoxy resins

Xin Wang [a,b], Weiyi Xing [a], Xiaming Feng [a], Bin Yu [a,b], Hongdian Lu [c], Lei Song [a,1], Yuan Hu [a,b,*]

[a] State Key Laboratory of Fire Science, University of Science and Technology of China, Anhui 230026, PR China
[b] Suzhou Key Laboratory of Urban Public Safety, Suzhou Institute for Advanced Study, University of Science and Technology of China, Suzhou, Jiangsu 215123, PR China
[c] Department of Chemical and Materials Engineering, Hefei University, Hefei, Anhui 230022, PR China

HIGHLIGHTS

- Adding metal oxide–graphene hybrids improved thermal stability of EP significantly.
- The barrier effect of graphene is the crucial factor for enhanced thermal stability.
- The organic volatiles and toxic CO are decreased during pyrolysis of the composite.
- The catalysis and adsorption effect of metal oxide/graphene are the mechanism of the smoke suppression.

ARTICLE INFO

ABSTRACT

Metal oxide decorated graphene hybrid materials, Co_3O_4–graphene and SnO_2–graphene, were synthesized for improving the thermal stability and suppressing the smoke in combustion for epoxy resins. Incorporation of metal oxide/graphene hybrids leads to significant thermal stabilization: a 37 and 27 °C increment in the temperature of 5% mass loss is observed for SnO_2–graphene/EP and Co_3O_4–graphene/EP, respectively, compared to that of pure EP. The barrier effect of graphene and the restricted mobility of the polymer chains by metal oxide are believed to be the crucial factor for improving the thermal stability. TG-FTIR analysis shows that the amount of organic volatiles of EP is significantly reduced and the toxic CO is suppressed after incorporating SnO_2–graphene or Co_3O_4–graphene, impling the reduced fire hazards. The synergism between the catalysis effect of metal oxide and the adsorption effect of graphene is the possible mechanism for the smoke suppression.

© 2014 Elsevier B.V. All rights reserved.

1. Introduction

Epoxy resin (EP), as a very important thermosetting polymer, has been widely used to manufacture high-performance composites in many fields such as aerospace structure materials, electronic laminate materials, and insulation materials due to its excellent adhesion, mechanical strength and solvent resistance [1–3]. However, like many synthetic polymers, there is one obvious disadvantage related to the high flammability of EP. The combustion of EP generates a large amount of heat and toxic smoke. Fire fatalities are usually reported as resulting from the lethal atmosphere generated by fires. Carbon monoxide concentrations measured in real fires can reach up to 7500 ppm [4], which would probably result in a loss of consciousness in 4 min [5]. A statistical study covering almost 5000 fatalities showed that the vast majority of fire deaths are attributable to carbon monoxide poisoning [6]. Therefore, it is of significant importance to improve the thermal stability and reduce the smoke toxicity of EP.

Graphene, a one-atom-thick carbon sheet with unique electronic and geometric properties, has been demonstrated to be one of the most promising candidates for the next generation of polymer nanocomposites. Small fraction of the graphene can lead to a significant improvement in thermal stability of polymers: the onset degradation temperature (T_{onset}) of the graphene/polystyrene is increased by approximately 60 °C at 0.19 vol% of graphene loading [7]; the addition of as low as 0.04 vol% graphene sheets leads to a 54 °C increase of T_{onset} for polyethylene [8]. Recently, graphene has been extensively investigated as a support for heterogeneous catalysts due to the ultrahigh aspect ratio for catalytic reaction [9]. Metal oxide/graphene hybrid materials are widely
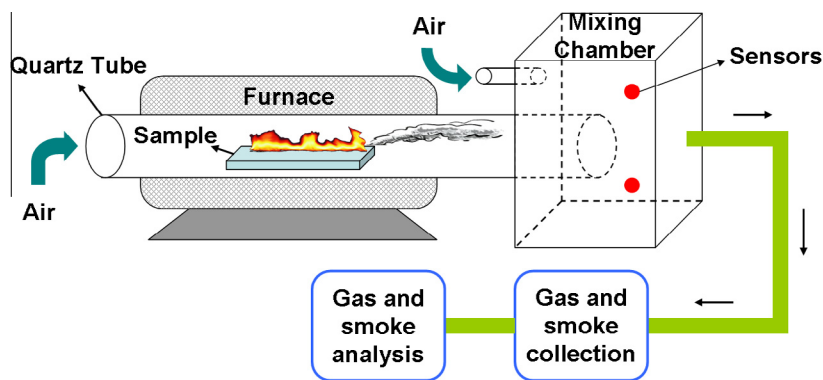
* Corresponding author at: State Key Laboratory of Fire Science, University of Science and Technology of China, Anhui 230026, PR China. Tel./fax: +86 551 63601664.
E-mail addresses: leisong@ustc.edu.cn (L. Song), yuanhu@ustc.edu.cn (Y. Hu).
1 Co-corresponding author: Tel./fax: +86 551 63601642.

Scheme 1. The diagrammatic illustration of the steady state tube furnace.

Fig. 1. The XRD patterns of graphene, Co_3O_4–graphene and SnO_2–graphene hybrids.

of the enhanced thermal stability of the composites and the reduced smoke toxicity was proposed. It is anticipated that metal oxide decorated graphene hybrid materials will provide a promising solution to reduce the fire hazards of polymers.

2. Experimental work

2.1. Materials

Graphite oxide (GO) was prepared from graphite using Hummers' method [14]. Cobalt acetate, $SnCl_4$, ethanol, ammonia and 4,4′-diamino diphenyl methane (DDM) were purchased from Sinopharm Chemical Reagent Co. Ltd (Shanghai, China). Biphenol A-type epoxy resin was supplied by Hefei Jiangfeng Chemical Industry Co. Ltd (Anhui, China). All the reagents were used as received without further purification. Deionized water was used for all experiments unless otherwise stated.

2.2. Synthesis of Co_3O_4–graphene and SnO_2–graphene hybrids

Co_3O_4–graphene hybrid was synthesized by a simple in situ chemical reduction process [15]. Firstly, 100 mg of GO was added to 400 ml of DI water with the assistance of sonication for 120 min. Then, 350 mg of cobalt acetate and 400 ml of DI water were added dropwise to the above graphene oxide solution. Meanwhile, 4 ml of ammonia was added to reduce cobalt ions and graphene oxide simultaneously. The solution was stirred for 4 h at 100 °C and the resulting precipitates were collected by filtration

used for the catalytic oxidation of carbon monoxide, such as CuO-embedded graphene [10], TiO_2-decorated graphene [11,12], Co_3O_4 supported on graphene sheets [13]. Furthermore, metal oxide nanoparticles are usually used in technology as absorbents, ion exchangers and catalysts.

In this work, Co_3O_4 and SnO_2 decorated graphene hybrids were synthesized and incorporated into epoxy matrix. The thermal stability and the smoke suppression of the Co_3O_4–graphene/EP and SnO_2–graphene/EP composites were investigated. The mechanism
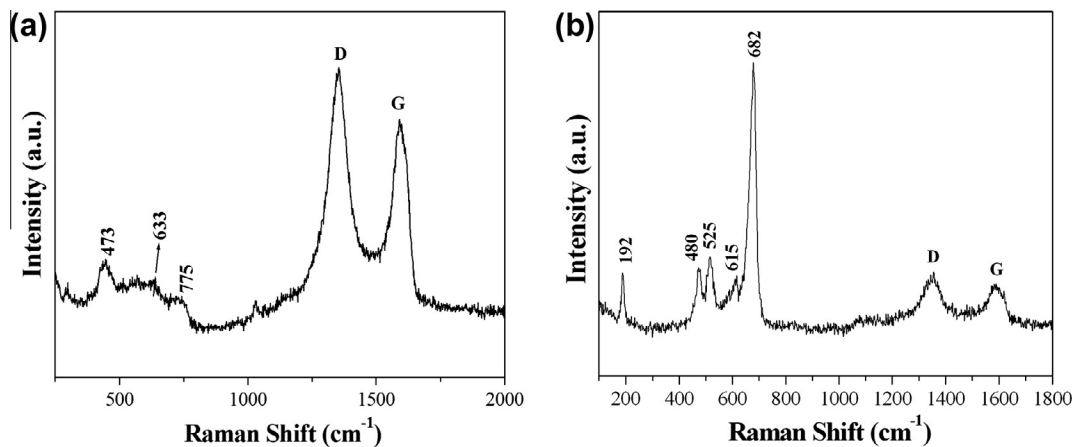

Fig. 2. The Raman spectra of (a) SnO_2–graphene and (b) Co_3O_4–graphene hybrids.

and subsequently oxidized at 400 °C, yielding the Co_3O_4–graphene hybrids.

To prepare the SnO_2–graphene, 0.25 g of GO was ultrasonically dispersed in 50 ml deionized water for 60 min, and then added to the 50 ml 0.04 M $SnCl_4$ ethanol solution. The suspension was reduced by 1 ml ammonia while it was vigorously stirred for 6 h. Then the precipitates were collected by centrifugation, washed several times with deionized water, dried and finally heated in a tube furnace at 400 °C for 1 h to obtain the SnO_2–graphene hybrid.

2.3. Preparation of Co3O4–graphene/EP and SnO2–graphene/EP composites

Briefly, the preparation of epoxy composite with 2 wt% Co_3O_4–graphene was depicted as follows: Co_3O_4–graphene (200 mg) was dispersed into acetone and sonicated until Co_3O_4–graphene completely dispersed to form a black suspension. Then, epoxy resins (7.6 g) and DDM (2.2 g) were added to the suspension above and stirred until homogeneous mixtures were obtained. The mixtures were heated in a vacuum oven at about 60 °C to remove solvent. Then, the samples were cured at 100 °C for 2 h and post-cured at 150 °C for 2 h. The SnO_2–graphene/EP composite with equivalent filler content was prepared under the similar processing conditions.

2.4. Characterization

Wide-angle X-ray diffraction patterns of the samples were recorded on an X-ray diffractometer (Rigaku Dmax/rA, Japan), using Cu K_α radiation ($k = 0.15418$ nm) at 40 kV and 20 mA. Raman
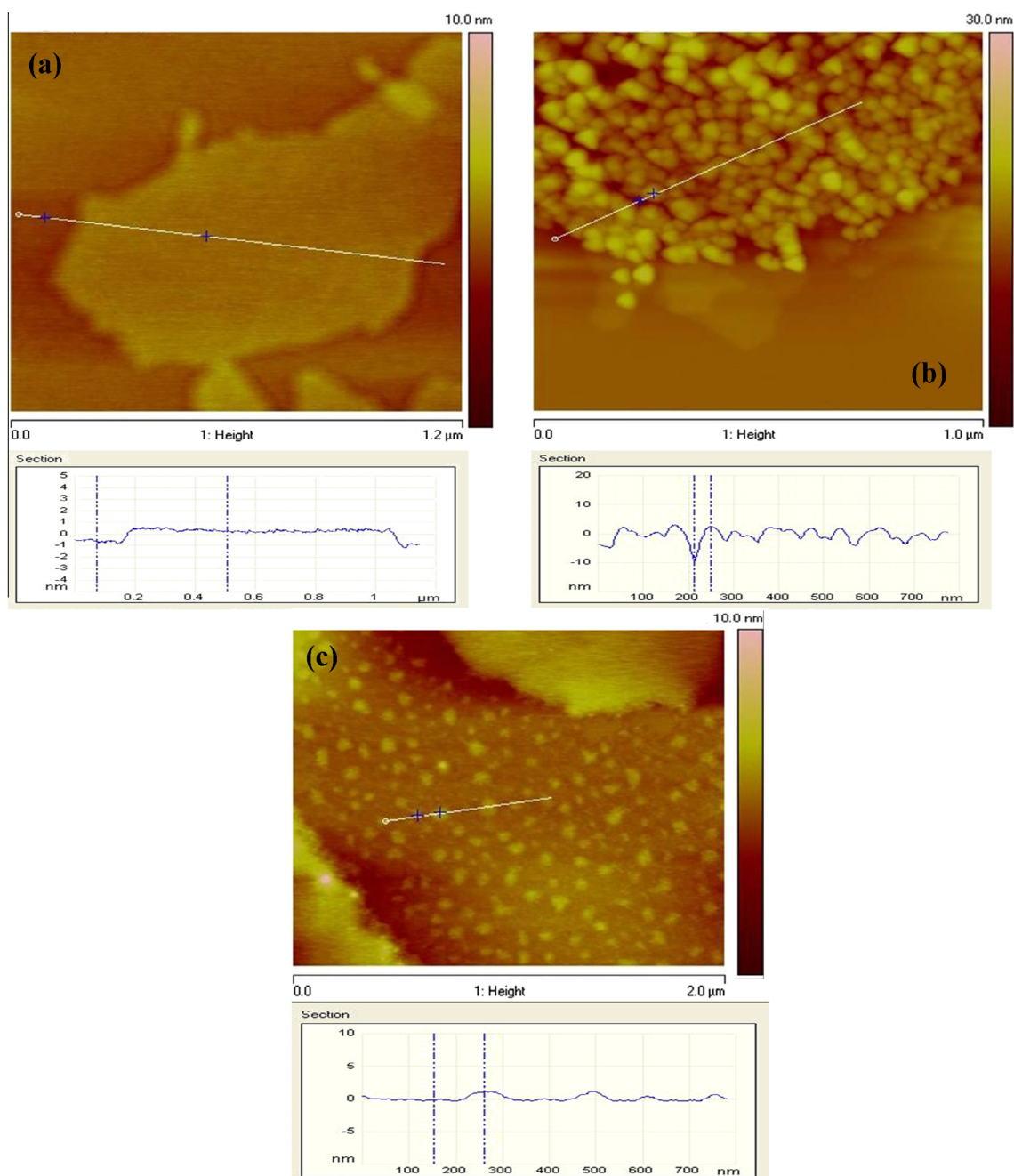

Fig. 3. AFM images of (a) graphene, (b) SnO_2–graphene and (c) Co_3O_4–graphene hybrids.

spectra were recorded from 100 to 2000 cm^{-1} on a LabRAM-HR Confocal Raman Microprobe (Jobin Yvon Instruments, France) using a 514.5 nm argon ion laser. Atomic force microscopy (AFM) observation was performed on the DI Multimode V in tapping-mode. The combustion properties were evaluated using a micro-scale combustion calorimeter (MCC, GOVMARK). The samples were tested according to ASTM D7309-07. Approximately 4 ± 1 mg of each sample was raised into the heated tube of a pyrolysis–combustion flow calorimeter (PCFC) that was purged with nitrogen. The sample was gradually heated to 650 °C at a heating rate of 1 °C s^{-1}. The gaseous pyrolysis products mix in the gas stream with oxygen prior to entering the combustion zone of the PCFC, where they are completely oxidized. Oxygen and nitrogen flow rates were set at 20 and 80 cm^3 min^{-1}, respectively. Values reported herein were the average of 3 tests. Thermogravimetric analysis (TGA) of samples were carried out with Q5000 thermal analyzer (TA Co., USA) from 50 °C to 700 °C at a heating rate of 20 °C/min in nitrogen atmosphere. The thermogravimetric analysis/infrared spectrometry (TG–IR) was performed using the TGA Q5000 IR thermogravimetric analyzer which was coupled with the Nicolet 6700 FT-IR spectrophotometer through a stainless steel transfer pipe. The pipe and gas cell were kept at 200 °C, to avoid the condensation of the volatile compounds. The fire toxicity was assessed using a steady state tube furnace (ISO TS 19700), as shown in Scheme 1. An amount of sample (about 20 g) in the form of granules or pellets, spread evenly along the quartz boat is introduced into a tube furnace at a constant rate. A current of air is passed through the furnace over the specimen to support combustion. The effluent is expelled from the tube furnace into a mixing chamber, where the carbon monoxide concentration and the smoke density can be measured.

3. Results and discussion

3.1. Structural and morphological characterization

The XRD patterns of graphene, Co_3O_4–graphene and SnO_2–graphene hybrids are presented in Fig. 1. The XRD trace of graphene powders exhibits a broad diffraction peak at 24.5°, which corresponds to the C(002) reflection of graphene. The major diffraction peaks of Co_3O_4–graphene are well indexed with the cubic spinel Co_3O_4, which are in good agreement with the standard card of Co_3O_4 (JCPDS card No. 42-1467) [16]. For SnO_2–graphene hybrid, all of the diffraction peaks could be assigned to rutile SnO_2 (JCPDS 41-1445) [17–19]. The diffraction peak of C(002) in graphene is invisible indicating that significant face-to-face stacking is broken due to the introduction of Co_3O_4 or SnO_2 nanoparticles. Additionally, no apparent additional peaks have been observed suggesting that Co_3O_4–graphene and SnO_2–graphene hybrids are of high purity.

The phases of SnO_2–graphene and Co_3O_4–graphene hybrids are further confirmed by Raman spectroscopy. The Raman spectra of SnO_2–graphene and Co_3O_4–graphene hybrids are presented in Fig. 2. In the spectra of SnO_2–graphene (Fig. 2a), the peaks detected at around 473, 633 and 775 cm^{-1} result from the rutile SnO_2 crystal, which are assigned to the E_g, A_{1g} and B_{2g} vibration mode, respectively [20,21]. In the spectra of Co_3O_4–graphene (Fig. 2b), the peaks at around 192, 480, 525, 615 and 682 cm^{-1} are assigned to E_g, F_{2m}^1, F_{2g}^2, and A_{1g} modes of Co_3O_4 [22,23]. For both the samples, two broad peaks at 1360 and 1595 cm^{-1} are observed, which are assigned to the D and G bands of graphene, respectively. The D band is attributed to the mode of the κ-point phonons of A_{1g} symmetry while the G band corresponds to the E_{2g} phonon of C_{sp2} atoms [24].

The morphology of graphene, SnO_2–graphene and Co_3O_4–graphene hybrids was characterized by AFM, as shown in Fig. 3.

From Fig. 3a, it can be clearly observed that graphene presents a nanoplatelet shape with several hundred nanometers large and 0.896 nm in thickness. In Fig. 3b, the SnO_2 nanoparticles (dark dot) are firmly attached to the surface of the graphene. The attached SnO_2 nanoparticles on the surface of graphene sheets heighten its thickness to about 11.588 nm, comparing to the thickness of graphene about 0.896 nm. In Fig. 3c, the cobalt oxide nanoparticles are uniformly displayed on the graphene sheets. Also, the height of the cobalt oxide particles on the graphene sheets is estimated from line scan profile to be about 2.5 nm. The well
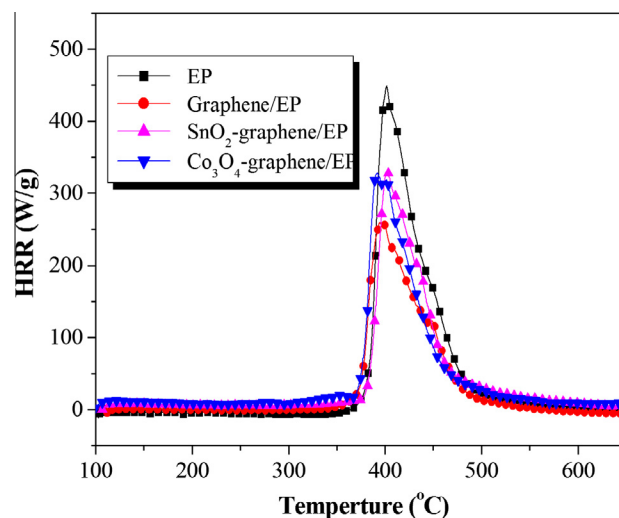

Fig. 4. The heat release rate (HRR) curves of pure EP, graphene/EP, SnO_2–graphene/EP and Co_3O_4–graphene/EP.

Table 1
MCC data of EP, graphene/EP, SnO_2–graphene/EP and Co_3O_4–graphene/EP.

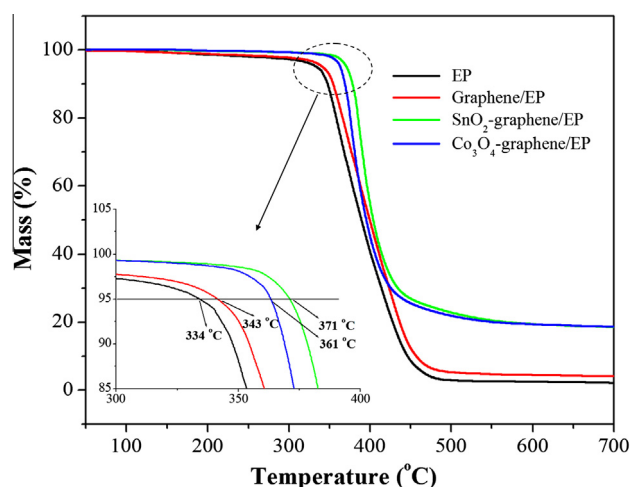| Sample	Peak HRR (W/g)	THR (kJ/g)	Char yield (%)
EP	449	24.4	10.6
Graphene/EP	285	20.3	15.3
SnO_2–graphene/EP	318	18.3	16.1
Co_3O_4–graphene/EP	329	20.3	13.0

Fig. 5. TGA profiles of pure EP, graphene/EP, SnO_2–graphene/EP and Co_3O_4–graphene/EP composites. Inset: enlarged curves of indicated region (by black circle).
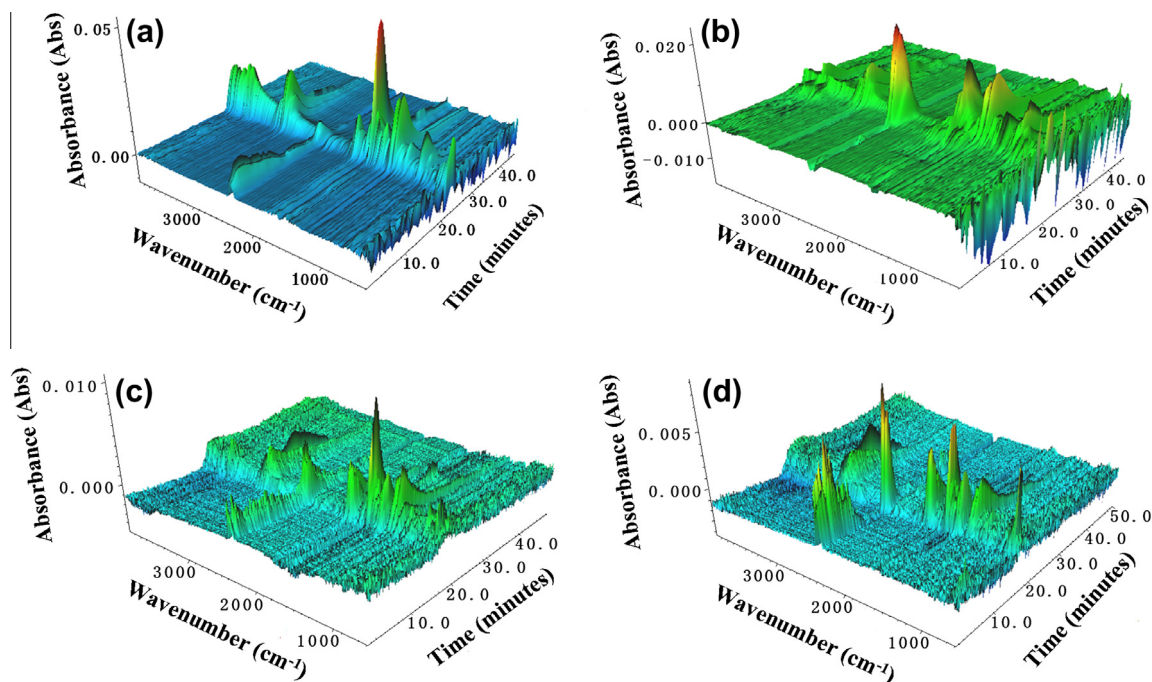
Fig. 6. The 3D diagrams of the gaseous volatiles during pyrolysis process of (a) pure EP, (b) graphene/EP, (c) SnO$_2$–graphene/EP and (d) Co$_3$O$_4$–graphene/EP composites.

dispersion of metal oxide nanoparticles on the graphene is probably attributed to that the presence of graphene with huge aspect ratio may prevent the nanoparticles from aggregation during preparation.

3.2. Flammability and thermal properties

MCC is a new, rapid laboratory scale test that measures flammability of materials on milligram quantities. The heat release rate (HRR) curves of pure EP, graphene/EP, SnO$_2$–graphene/EP and Co$_3$O$_4$–graphene/EP are shown in Fig. 4 and some important parameters obtained from the MCC tests, such as the peak heat release rate (PHRR), the total heat release (THR) and the char yield, are listed in Table 1. It can be observed that pure EP burns very rapidly after ignition and the peak heat release rate value is 449 W g^{-1}. As expected, the addition of graphene, SnO$_2$–graphene and Co$_3$O$_4$–graphene gives rise to a 36%, 29% and 27% reduction in PHRR, respectively, compared to that of pure EP. These results indicate that the barrier effect of graphene plays an important role in reducing the heat release rate. Furthermore, incorporating graphene, SnO$_2$–graphene and Co$_3$O$_4$–graphene into EP also leads to the reduction in THR and the increment in char yield. The mechanism of metal oxide decorated graphene hybrids in reducing the flammability of EP is probably attributed to the higher char yield which could retard the heat and mass transfer between gas and polymers.

Fig. 5 depicts TGA profiles of pure EP, graphene/EP, SnO$_2$–graphene/EP and Co$_3$O$_4$–graphene/EP composites under nitrogen atmosphere. The onset degradation temperature (T_{onset}) is defined as the temperature at which the mass loss is 5%. As can be observed, the thermal degradation process of pure EP mainly has a single stage in the temperature range from 300 to 500 °C, which corresponds to the decomposition of the macromolecular networks. The degradation behavior of graphene/EP, SnO$_2$–graphene/EP and Co$_3$O$_4$–graphene/EP composites is similar to that of pure EP. However, the thermal stability of graphene/EP is enhanced compared with that of the neat EP. It is proposed that the so-called "tortuous path" effect of graphene is one of the reasons for the significant
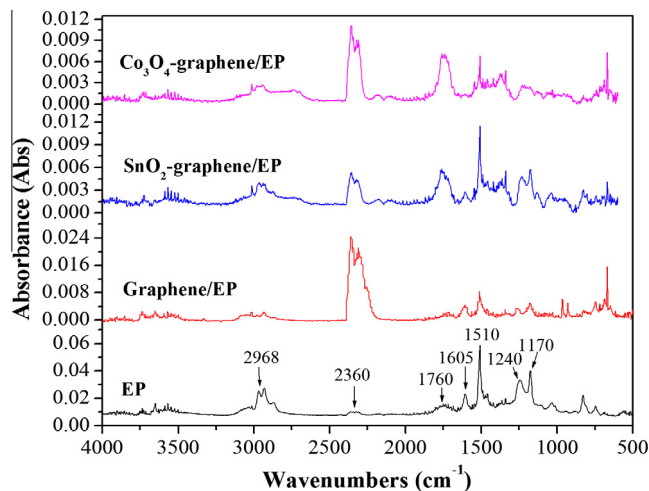

Fig. 7. FTIR spectra of pyrolysis products of EP, graphene/EP, SnO$_2$–graphene/EP and Co$_3$O$_4$–graphene/EP composites at maximum decomposition rates.

improvement in thermal stability, because the barrier action retards the permeation of heat and the escape of volatile degradation products [25]. Furthermore, a 37 and 27 °C increment in T_{onset} is observed for SnO$_2$–graphene/EP and Co$_3$O$_4$–graphene/EP, respectively, compared to that of pure EP. The stabilizing mechanism of SnO$_2$–graphene and Co$_3$O$_4$–graphene is similar, which could be attributed to the synergistic effect between metal oxide particles (steric hindrance and surface adsorption of the polymer chains to restrict their mobility as previously reported [26,27]) and graphene (physical barrier effect).

3.3. Smoke toxicity and suppression

To investigate the effect of metal oxide decorated graphene hybrid materials on the evolved gas products during pyrolysis,

TG-FTIR was employed to analyze the volatile components of EP, graphene/EP, SnO_2–graphene/EP and Co_3O_4–graphene/EP composites. Fig. 6 displays the 3D diagrams of EP, graphene/EP, SnO_2–graphene/EP and Co_3O_4–graphene/EP composites. It can be observed that the typical thermal degradation process of the composites is similar to pure EP. The characteristic peaks appear in the regions of 3600–3700, 2750–3150, 2250–2400, 1400–1650, and 1100–1300 cm^{-1}.

In order to provide a clear comparison, FTIR spectra of pyrolysis products of EP, graphene/EP, SnO_2–graphene/EP and Co_3O_4–graphene/EP composites at maximum decomposition rates are presented in Fig. 7. As can be seen, the similar characteristic peaks in the FTIR spectra of the samples indicate the similar composition of the gaseous products. Some of the gaseous pyrolysis products of the EP materials were unambiguously identified by characteristic strong FTIR signals: the bands at 3450–3600 cm^{-1} are due to the vibration absorption of hydroxide groups, indicating the generation of water; the characteristic bands at 2950–2850 and 1100–1300 cm^{-1} are corresponding to the vibration absorption of $-CH_3$ and $-CH_2-$ groups in various hydrocarbons; the bands at 2360 and 2190 cm^{-1} are assigned to the absorbance of carbon dioxide and carbon monoxide, respectively; the characteristic peak at 1760 cm^{-1} is due to the absorbance of stretching vibration of C=O group; and the peaks at 1605, 1510 cm^{-1} are ascribed to the characteristic bands of aromatic rings [28–30]. It can be seen that the relative intensity of characteristic peak of carbon dioxide at 2360 cm^{-1} is increased for the composites as compared to that of pure EP, suggesting that the flammable gases may be diluted by the nonflammable CO_2 in the gas phase [31]. Therefore, it is possible that the thermal degradation may be retarded.

To further understand the changes of the pyrolysis products, the absorbance of four selected gas products for EP, graphene/EP, SnO_2–graphene/EP and Co_3O_4–graphene/EP composites versus temperature is revealed in Fig. 8. It can be clearly seen that the addition of graphene decreases the maximum absorbance intensity of the pyrolysis products of epoxy resins, which is attributed to that the physical barrier effect of graphene retards the permeation of heat and the escape of volatile degradation products. Moreover, the maximum absorbance intensity of the pyrolysis products for SnO_2–graphene/EP and Co_3O_4–graphene/EP composites is much lower than that for EP, especially for carbonyl and aromatic compounds. The reduced amount of the organic volatiles results in the reduced heat release rate, because most of the organic volatiles are flammable gases as "fuel" during combustion. The reduced amount of the organic volatiles further leads to the inhibition of smoke, since the organic volatiles are the major source of smoke particles [32]. Additionally, CO production for SnO_2–graphene/EP and Co_3O_4–graphene/EP composites is also much lower than that of pure EP. The reduction of CO gives rise to the decrease in the smoke toxicity during combustion, which will be beneficial for fire rescue when an accident happens.

The steady state tube furnace has been developed specifically to evaluate the generation of toxic products from real fires on a bench-scale in recent years [33]. Fig. 9 presents the CO yield and the smoke density versus time curves of EP, graphene/EP, SnO_2/EP, Co_3O_4/EP, SnO_2–graphene/EP and Co_3O_4–graphene/EP composites. As can be observed from Fig. 9, graphene/EP exhibits a slightly reduced CO concentration and smoke density compared to those of pure EP, because graphene only functions as the physical adsorption effect due to its huge specific surface area. Also, adding SnO_2
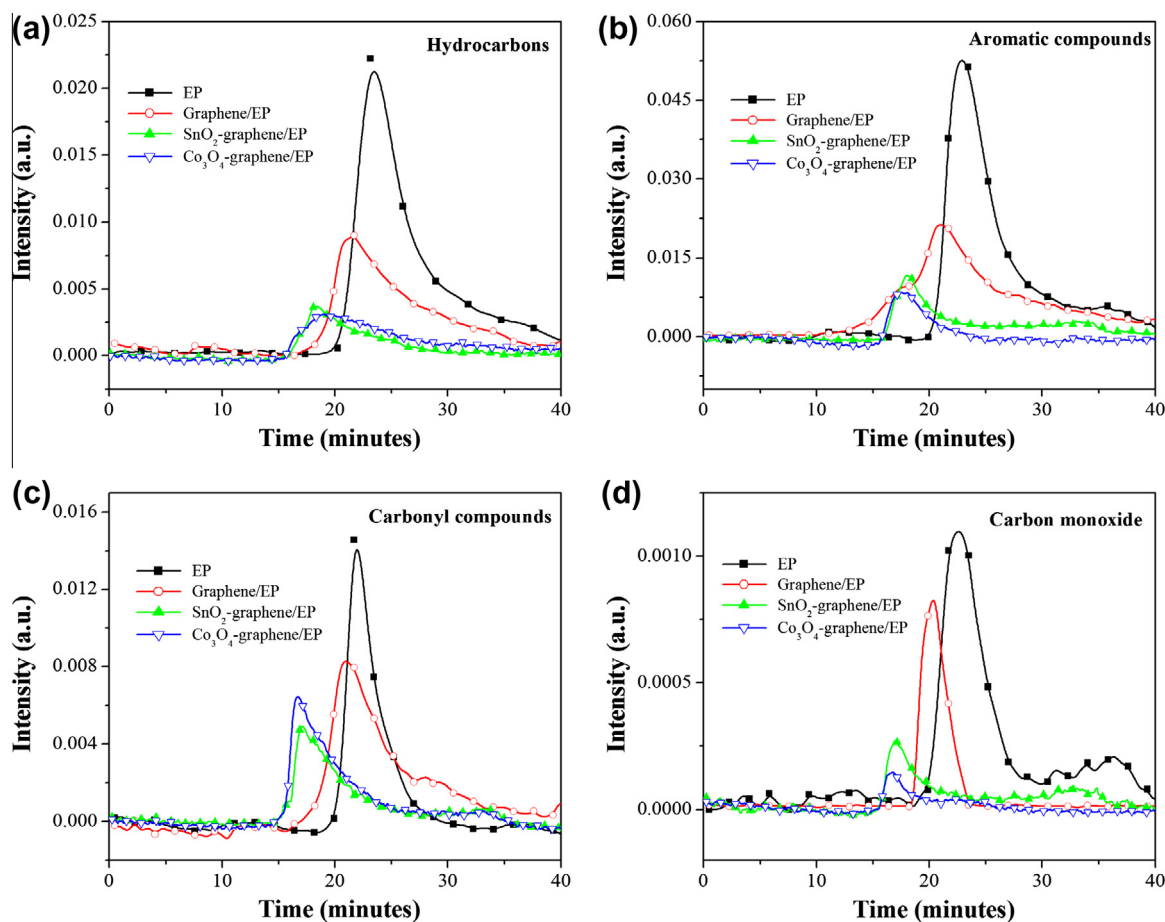

Fig. 8. Intensity of characteristic peaks for pyrolysis products of EP, graphene/EP, SnO_2–graphene/EP and Co_3O_4–graphene/EP composites.
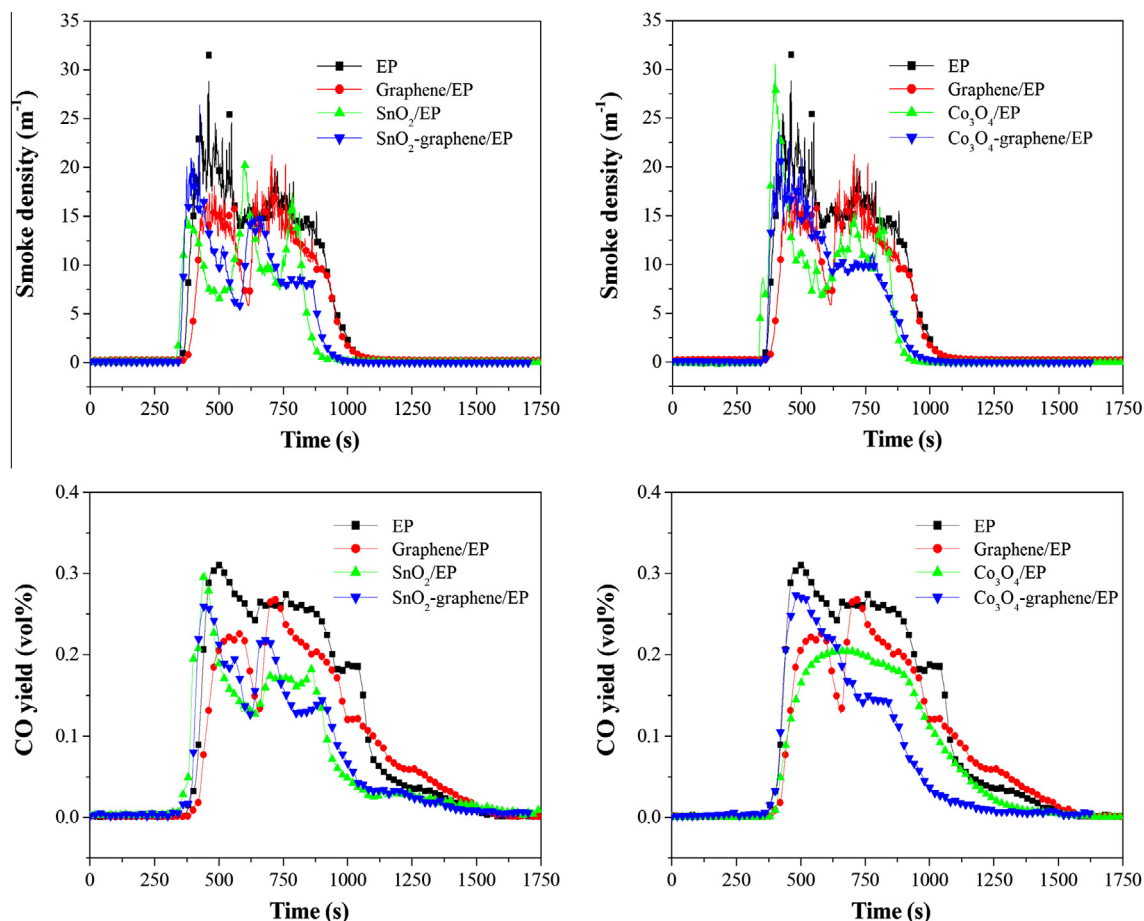
Fig. 9. The CO yield and the smoke density versus time curves of EP, graphene/EP, SnO2/EP, Co3O4/EP, SnO2–graphene/EP and Co3O4–graphene/EP composites.

or Co_3O_4 into EP decreases the CO concentration and the smoke density of polymer composites owing to the catalysis effect of metal oxide. The CO molecule is absorbed by the Co^{3+} cation in Co_3O_4 and then the adsorbed CO is oxidized by abstracting the surface oxygen that might be coordinated with three Co^{3+} cations [34]; similarly, SnO_2 is also reported as an effective catalyst for the oxidation of carbon monoxide [35]. Moreover, the incorporation of SnO_2–graphene or Co_3O_4–graphene effectively decreases the CO concentration and the smoke density during combustion, which is attributed to the synergism of the catalysis effect of metal oxide and the adsorption effect of graphene. Graphene is apt to absorb the small gaseous molecules so that retards the escape of the organic volatiles to form smoke, while the metal oxide particles catalyze the oxidation of CO to reduce the smoke toxicity.

In summary, the possible mechanisms of the improved thermal stability and the reduced smoke toxicity of metal oxide–graphene/ EP are proposed as follows: (i) the "tortuous path" effect of graphene and the restricted mobility of the polymer chains by metal oxide play a synergistic role in improving the thermal stability; (ii) the synergism between the catalysis effect of metal oxide and the adsorption effect of graphene is responsible for the reduction of the heat release rate and the smoke toxicity. In addition, the thermal stability and the smoke suppression effect of SnO_2–graphene/EP are superior to those of Co_3O_4–graphene/EP, which could be explained by that tin dioxide appears to operate in both the condensed phase mechanism involving the promotion of char formation and the gaseous phase flame inhibition, while cobaltosic oxide functions mainly in the condensed phase [36].

4. Conclusion

In conclusion, SnO_2–graphene and Co_3O_4–graphene hybrid materials were successfully synthesized and applied into flame retardant epoxy resins as well as smoke suppressant. TGA results shows that the thermal stability of EP is significantly enhanced by incorporating SnO_2–graphene and Co_3O_4–graphene at a low loading (2 wt%). The "barrier" effect of graphene is believed to be an important factor to the enhanced thermal stability of the composites. Due to the synergism between the catalysis effect of metal oxide and the adsorption effect of graphene, the amount of the harmful organic volatiles and the toxic CO is reduced, and the relative intensity of the nonflammable CO_2 is increased. The reduced "fuel" and the dilution of the flammable gases by CO_2 are the main reasons for the decreased PHRR and THR, which is in good accordance with the MCC results. It is anticipated that metal oxide decorated graphene hybrid materials will provide a promising solution to flame retardant polymers with enhanced thermal stability and low smoke toxicity.

References

[1] B. Perret, B. Schartel, K. Stoss, M. Ciesielski, J. Diederichs, M. Doring, J. Kramer, V. Altstadt, Novel DOPO-based flame retardants in high-performance carbon fibre epoxy composites for aviation, Eur. Polym. J. 47 (2011) 1081–1089.

[2] J. Artner, M. Ciesielski, O. Walter, M. Doring, R.M. Perez, J.K.W. Sandler, V. Altstadt, B. Schartel, A novel DOPO-based diamine as hardener and flame retardant for epoxy resin systems, Macromol. Mater. Eng. 293 (2008) 503–514.

[3] K. Wu, B.K. Kandola, E. Kandare, Y.A. Hu, Flame retardant effect of polyhedral oligomeric silsesquioxane and triglycidyl isocyanurate on glass fibre-reinforced epoxy composites, Polym. Composite 32 (2011) 378–389.

[4] J.H. Troitzsch, Fire gas toxicity and pollutants in fires: the role of flame retardants, in: Flame Retardants 2000. Interscience Communications, London, 2000, pp. 177–184.

[5] D.J. Irvine, J.A. McCluskey, I.M. Robinson, Fire hazards and some common polymers, Polym. Degrad. Stab. 67 (2000) 383–396.

[6] M.M. Hirschler, Fire retardance, smoke toxicity and fire hazard, in: Flame Retardants '94. Interscience Communications, London, 1994, pp. 225–238.

[7] V.H. Pham, T.V. Cuong, T.T. Dang, S.H. Hur, B.S. Kong, E.J. Kim, E.W. Shin, J.S. Chung, Superior conductive polystyrene-chemically converted graphene nanocomposite, J. Mater. Chem. 21 (2011) 11312–11316.

[8] S. Cheng, X. Chen, Y.G. Hsuan, C.Y. Li, Reduced graphene oxide-induced polyethylene crystallization in solution and nanocomposites, Macromolecules 45 (2012) 993–1000.

[9] D.W. Boukhvalov, M.I. Katsnelson, Enhancement of chemical activity in corrugated graphene, J. Phys. Chem. C 113 (2009) 14176–14178.

[10] W.Y. Li, Q.L. Chen, W. Qin, N. Wang, J.L. Lai, Interaction of CO with CuO and CuO/graphene: reactions mechanism and the formation of CO_2, Adv. Mater. Res. – Switz. 354–355 (2012) 279–285.

[11] G. Williams, B. Seger, P.V. Kamat, TiO_2–graphene nanocomposites. UV-assisted photocatalytic reduction of graphene oxide, ACS Nano 2 (2008) 1487–1491.

[12] X.Y. Zhang, H.P. Li, X.L. Cui, Y.H. Lin, Graphene/TiO_2 nanocomposites: synthesis, characterization and application in hydrogen evolution from water photocatalytic splitting, J. Mater. Chem. 20 (2010) 2801–2806.

[13] X. Wang, L. Song, H.Y. Yang, W.Y. Xing, H.D. Lu, Y. Hu, Cobalt oxide/graphene composite for highly efficient CO oxidation and its application in reducing the fire hazards of aliphatic polyesters, J. Mater. Chem. 22 (2012) 3426–3431.

[14] W.S. Hummers, R.E. Offeman, Preparation of graphitic oxide, J. Am. Chem. Soc. 80 (1958) 1339.

[15] H. Kim, D.H. Seo, S.W. Kim, J. Kim, K. Kang, Highly reversible Co_3O_4/graphene hybrid anode for lithium rechargeable batteries, Carbon 49 (2011) 326–332.

[16] S.B. Yang, G.L. Cui, S.P. Pang, Q. Cao, U. Kolb, X.L. Feng, J. Maier, K. Mullen, Fabrication of cobalt and cobalt oxide/graphene composites: towards high-performance anode materials for lithium ion batteries, Chemsuschem 3 (2010) 236–239.

[17] B. Cheng, J.M. Russell, W.S. Shi, L. Zhang, E.T. Samulski, Large-scale, solution-phase growth of single-crystalline SnO_2 nanorods, J. Am. Chem. Soc. 126 (2004) 5972–5973.

[18] D.L. Chen, L. Gao, Facile synthesis of single-crystal tin oxide nanorods with tunable dimensions via hydrothermal process, Chem. Phys. Lett. 398 (2004) 201–206.

[19] G.D. Zhang, N.A. Liu, Z.Y. Ren, B. Yang, Synthesis of high-purity SnO_2 nanobelts by using exothermic reaction, J. Nanomater. 2011 (2011) 526094.

[20] I.I. Gontia, M. Baibarac, I. Baltog, Photoluminescence and Raman studies on tin dioxide powder and tin dioxide/single-walled carbon-nanotube composites, Phys. Status Solidi B 248 (2011) 1494–1498.

[21] S.H. Sun, G.W. Meng, G.X. Zhang, T. Gao, B.Y. Geng, L.D. Zhang, J. Zuo, Raman scattering study of rutile SnO_2 nanobelts synthesized by thermal evaporation of Sn powders, Chem. Phys. Lett. 376 (2003) 103–107.

[22] J. Jiang, L.C. Li, Synthesis of sphere-like Co_3O_4 nanocrystals via a simple polyol route, Mater. Lett. 61 (2007) 4894–4896.

[23] H.C. Liu, S.K. Yen, Characterization of electrolytic Co_3O_4 thin films as anodes for lithium-ion batteries, J. Power Sources 166 (2007) 478–484.

[24] F. Tuinstra, J.L. Koenig, Raman spectrum of graphite, J. Chem. Phys. 53 (1970) 1126.

[25] Y.W. Cao, J.C. Feng, P.Y. Wu, Preparation of organically dispersible graphene nanosheet powders through a lyophilization method and their poly(lactic acid) composites, Carbon 48 (2010) 3834–3839.

[26] A. Laachachi, M. Cochez, E. Leroy, M. Ferriol, J.M. Lopez-Cuesta, Fire retardant systems in poly(methylmethacrylate): Interactions between metal oxide nanoparticles and phosphinates, Polym. Degrad. Stab. 92 (2007) 61–69.

[27] A. Laachachi, M. Cochez, M. Ferriol, J.M. Lopez-Cuesta, E. Leroy, Influence of TiO_2 and Fe_2O_3 fillers on the thermal properties of poly(methyl methacrylate) (PMMA), Mater. Lett. 59 (2005) 36–39.

[28] U. Braun, A.I. Balabanovich, B. Schartel, U. Knoll, J. Artner, M. Ciesielski, M. Doring, R. Perez, J.K.W. Sandler, V. Altstadt, T. Hoffmann, D. Pospiech, Influence of the oxidation state of phosphorus on the decomposition and fire behaviour of flame-retarded epoxy resin composites, Polymer 47 (2006) 8495–8508.

[29] K. Wu, L. Song, Y. Hu, H.D. Lu, B.K. Kandola, E. Kandare, Synthesis and characterization of a functional polyhedral oligomeric silsesquioxane and its flame retardancy in epoxy resin, Prog. Org. Coat. 65 (2009) 490–497.

[30] K. Wu, Y. Hu, L. Song, H.D. Lu, Z.Z. Wang, Flame retardancy and thermal degradation of intumescent flame retardant starch-based biodegradable composites, Ind. Eng. Chem. Res. 48 (2009) 3150–3157.

[31] T. Rajkumar, C.T. Vijayakumar, P. Sivasamy, B. Sreedhar, C.A. Wilkie, Thermal degradation studies on PMMA-HET acid based oligoesters blends, J. Therm. Anal. Calorim. 100 (2010) 651–660.

[32] Y.Y. Dong, Z. Gui, Y. Hu, Y. Wu, S.H. Jiang, The influence of titanate nanotube on the improved thermal properties and the smoke suppression in poly(methyl methacrylate), J. Hazard. Mater. 209 (2012) 34–39.

[33] A.A. Stec, T.R. Hull, K. Lebek, Characterisation of the steady state tube furnace (ISO TS 19700) for fire toxicity assessment, Polym. Degrad. Stab. 93 (2008) 2058–2065.

[34] X.W. Xie, Y. Li, Z.Q. Liu, M. Haruta, W.J. Shen, Low-temperature oxidation of CO catalysed by Co_3O_4 nanorods, Nature 458 (2009) 746–749.

[35] A. Boulahouache, G. Kons, H.G. Lintz, P. Schulz, Oxidation of carbon-monoxide on platinum tin dioxide catalysts at low-temperatures, Appl. Catal. A – Gen. 91 (1992) 115–123.

[36] P.A. Atkinson, P.J. Haines, G.A. Skinner, The mechanism of action of tin compounds as flame retardants and smoke suppressants for polyester thermosets, Polym. Degrad. Stab. 71 (2001) 351–360.